ELSEVIER

Engineering Geology 66 (2002) 111–125

ENGINEERING GEOLOGY

www.elsevier.com/locate/enggeo

Weathering mechanisms and their effects on the landsliding of ignimbrite subject to vapor-phase crystallization in the Shirakawa pyroclastic flow, northern Japan

M. Chigira [a,*], M. Nakamoto [b,1], E. Nakata [c]

[a] *Disaster Prevention Research Institute, Kyoto University, Gokasho, Uji 611-0011 Japan*
[b] *Graduate School of Science, Kyoto University, Yoshida-Honmachi, Sakyo, Kyoto 606-01 Japan*
[c] *Central Research Institute of Electric Power Industry, 1646, Abiko, Chiba 270-11 Japan*

Accepted 18 January 2002

Abstract

Ignimbrite, which is consolidated by vapor-phase crystallization, is weathered in humid regions to form a special type of weathering profile that consists of a hydrated zone, an exfoliated zone, and a disintegrated zone from the depth to the ground surface, with each zone having a basal front. The ignimbrite is hydrated first and loses a significant amount of phosphorous at the hydration front, where rock-forming tridymite is dissolved and cristobalite is precipitated. The ignimbrite further loses its alkali and alkali earth components at the top of the hydrated zone by reacting with reactive water from the exfoliated zone, then the leached layers are exfoliated and become part of the exfoliated zone, and then they soften significantly. At the top of the exfoliated zone, rock is disintegrated so completely that rock texture disappears. Water from rainstorms infiltrates down to the exfoliation front, but penetrates only slightly further downward, thus saturating the weathered rock in the exfoliated and disintegrated zones and leading to a landslide with a slip surface within the exfoliated zone.

Keywords: Ignimbrite; Pyroclastic flow; Vapor-phase crystallization; Weathering; Landslide

1. Introduction

Pyroclastics are widely distributed in tectonically active regions with volcanism (Cas and Wright, 1996). A pyroclastic flow deposit (i.e., ignimbrite), one of the most common pyroclastics, has been prone to landslides during heavy rainfalls. Shirasu, a typical non-welded and unconsolidated ignimbrite (age 24,500 years before the present; Yokoyama, 1999), has been subject to shallow landslides on many occasions, resulting in numerous casualties in Kagoshima Prefecture in southern Japan (Fig. 1) (Yokota and Iwamatsu, 1999; Yokoyama, 1999). Shirasu weathers so quickly that after a landslide strips off the weathered material, weathering recommences and quickly provides material for the next landslide (Shimokawa et al., 1989; Yokota and Iwamatsu, 1999). The migration of

* Corresponding author. Tel.: +81-774-38-4100; fax: +81-774-38-4105.
E-mail addresses: chigira@slope.dpri.kyoto-u.ac.jp (M. Chigira), nakamoto@slope.dpri.kyoto-u.ac.jp (M. Nakamoto), nakata@criepi.denken.or.jp (E. Nakata).
[1] Fax: +81-774-38-4105.

0013-7952/02/$ - see front matter
PII: S0013-7952(02)00035-2

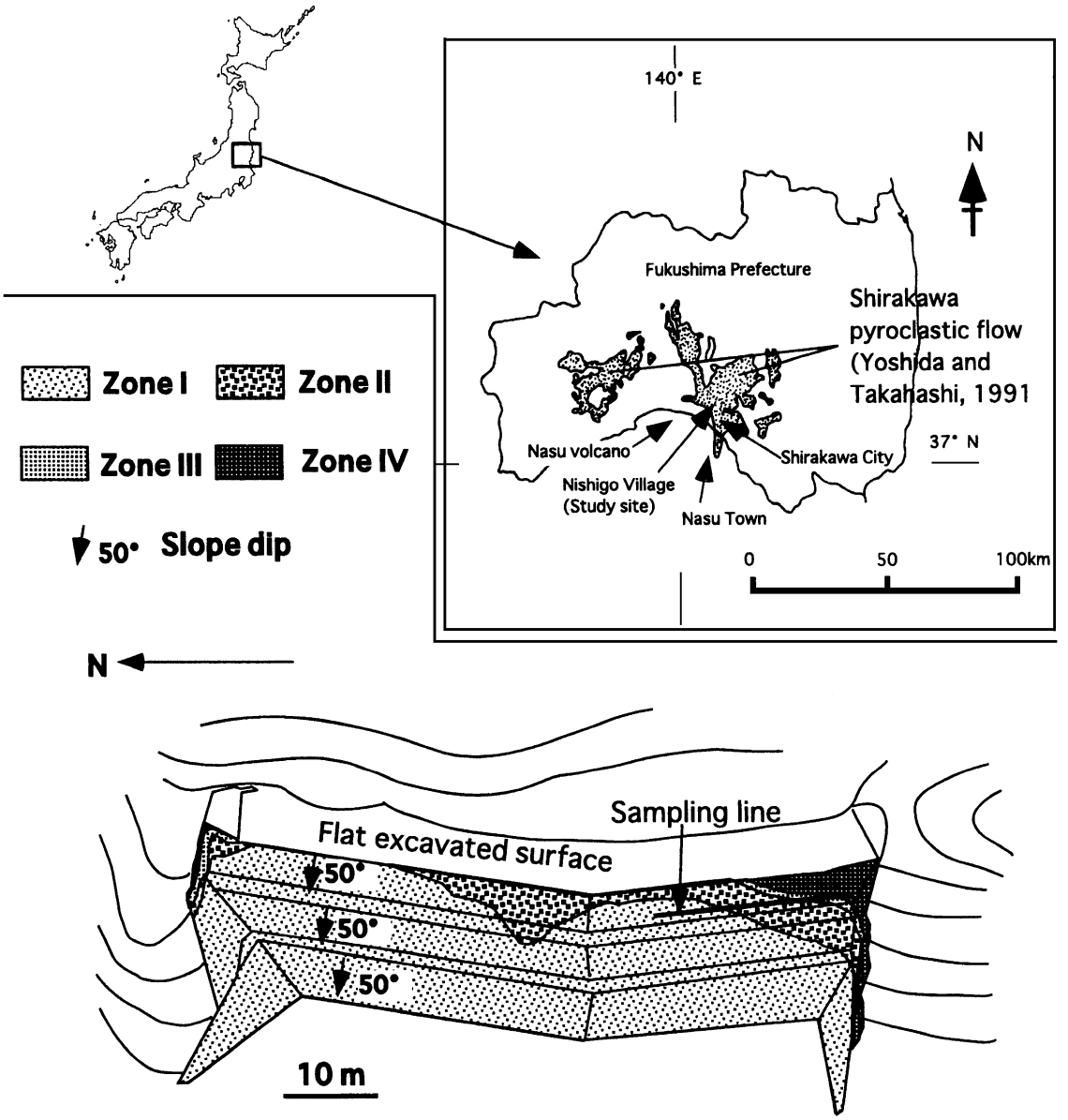

Fig. 1. Sketch of a typical weathering profile of vapor-phase crystallized ignimbrite of the Shirakawa pyroclastic flow.

a weathering front and the deterioration within the weathering zone proceed on the order of years, and the recurrence interval of landslides is on the order of tens of years to a few hundred years (Shimokawa et al., 1989). This weathering mechanism has not been elucidated sufficiently, but it is supposed that it is dominated by chemical processes involving the interaction between Shirasu and groundwater. Such a mechanism is indicated by the increase in water content toward the ground surface and the formation of halloysite (Shimokawa et al., 1989; Yokota and Iwamatsu, 1999).

Ignimbrite that has been consolidated by vapor-phase crystallization, which hereafter will be referred

to as vapor-phase-consolidated ignimbrite, when it occurs in the outer zones of welded ignimbrite (Smith and Bailey, 1966; Best and Christinsen, 2001), is not as easily weathered as Shirasu, and reportedly has not been subject to landslides caused by heavy rainfall. In addition, the weathering profile of vapor-phase-consolidated ignimbrite has not been studied before. However, a rainstorm in August 1998 in northern Japan triggered numerous landslides in a region of vapor-phase consolidated ignimbrite.

This paper characterizes the weathering profile of vapor-phase-consolidated ignimbrite, clarifies its formative mechanism and discusses its role in the disintegration process of slopes consisting of that type of ignimbrite using the Quaternary Shirakawa pyroclastic flow as an example.

Heavy rainfall occurred in northern Japan from 26 to 31 August in 1998, causing a severe disaster involving floods and landslides. The rainfall was particularly strong in Nishigo Village, Shirakawa City and Nasu Town, with an hourly precipitation of 60 mm or more (Fig. 1). The cumulative rainfall in these areas exceeded 1200 mm, while monthly precipitation in August from 1979 to 1990 averaged from 200 to 280 mm (Ushiyama, 1999). This rainfall generated more than 1000 landslides within an area of 100 km^2 of ignimbrite. There were three types of landslides, the most dominant of which were landslides of heavily weathered ignimbrite with a slip surface within an exfoliated zone of the weathering zone (Chigira and Inokuchi, in press). The exfoliated zone is described and discussed in the context of weathering in the following sections.

2. Geological setting

The bedrock of the study site is the early Quaternary Shirakawa pyroclastic flow (Yoshida and Takahashi, 1991; Suzuki et al., 1998) overlain by thin beds of pyroclastics, which are supposed to have erupted from Nasu Volcano between 350,000 and 200,000 years ago (Suzuki, 1999). The Shirakawa pyroclastic flow has been divided into several flow units (Yoshida and Takahashi, 1991; Saotome et al., 1999). According to their classification, the flow of the study site belongs to the Nishigo pyroclastic flow, which is dated to be 780 ka (Yoshida and Takahashi, 1991; Suzuki et al., 1998), or the Rakuoukei pyroclastic flow (Saotome et al., 1999). The Shirakawa pyroclastic flow in the study site consists of white tuff, which is dacitic and poor in lithic and essential fragments, and contains pseudomorphs of high quartz with diameters of up to 3 mm, hornblende, pyroxene, tridymite and cristobalite. This is massive, intact tuff, which has no conspicuous glass lenses or joints but is estimated to have uniaxial compression strength of several MPa. It is essentially impermeable, with permeabilities on the order of 10^{-8} m/s, which was obtained by flow pump method developed by Olsen et al. (1985). Our preliminary survey of the Shirakawa pyroclastic flow in Nishigo Village indicates that most of it has similar properties to vapor-phase-consolidated ignimbrite such as that in the study site, which is lithified by the precipitation of tridymite and cristobalite. Heavily welded tuff with columnar joints or non-welded, sand-like ignimbrite only occur locally in Nishigo Village.

3. Methods

Characteristic and typical weathering profiles of the Shirakawa pyroclastic flow were found at three artificially cut slopes, and one of them was analyzed in detail (Figs. 1 and 2). The cut slope was made 3 years before the sampling. The weathering profile was divided into three zones according to color, structure, hardness and morphology of the cut surface (Fig. 1). These zones were temporarily named zones II, III and IV from the depth to the ground surface, with zone I being the unweathered zone. The boundaries among these zones were roughly parallel to the slope surface before cutting.

Zone I is characterized by massive, gray and relatively hard rock that retains scars made by excavating machines on its cut surface. Machine scars were preserved on the cut surface of the rock only in this zone. Zone II is characterized by massive, pale gray and relatively soft rock. The boundary between zones II and I is not very well defined, but is within an interval of 10–20 cm. The top of zone II is soft and partly creamy brown, an area which is a transitional zone to zone III, as will be discussed below. This transitional zone is less than ten centimeters thick, and its lower boundary is roughly parallel to its upper planar margin, the boundary with zone III. The boundary between zones II and

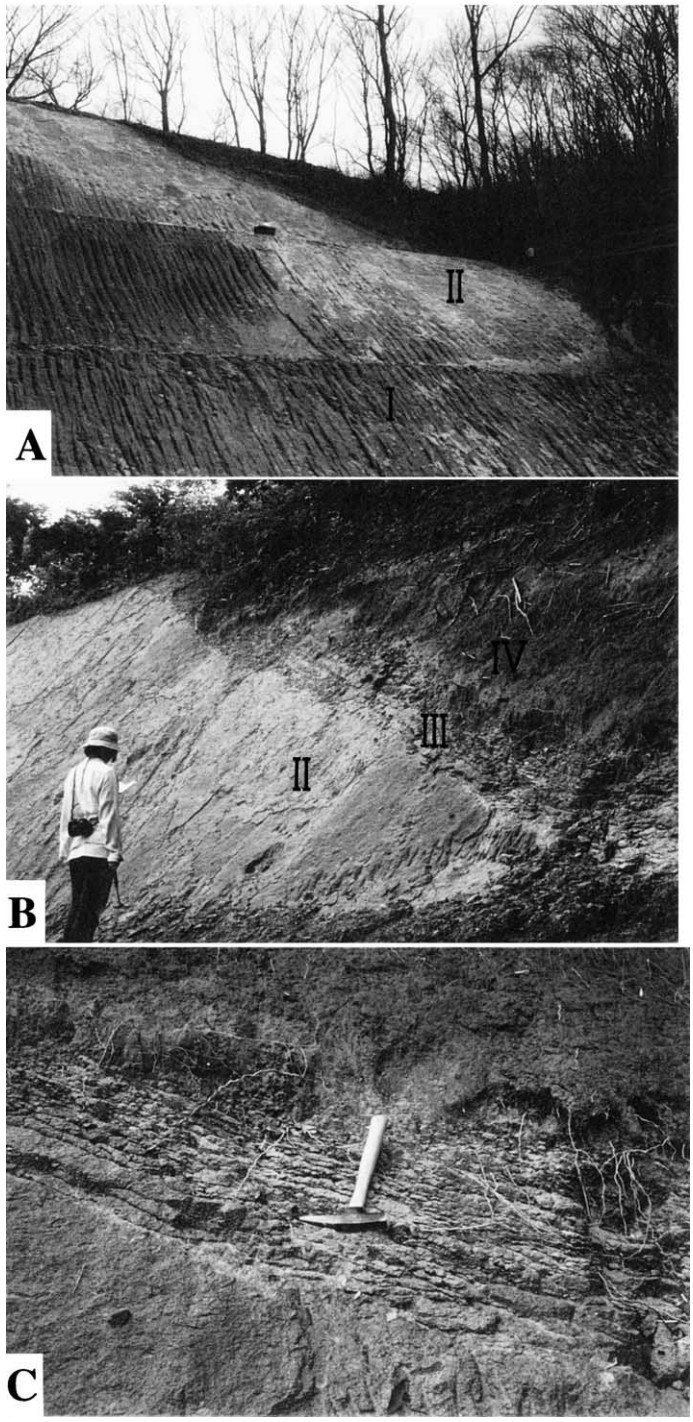

Fig. 2. Photographs of the outcrop of a cross section of a typical weathering profile, where the samples were taken. (A) Overview. (B) Zones I, II and III. (C) Close up of zone III, where rock is separated into platy segments.

III is clearly defined and is nearly planar. Zone III is characterized by pale gray or creamy brown and soft rock separated into platy segments that are roughly parallel to the boundary with the underlying zone II. The fractures separating the segments are undulating and anastomosing; the segments are a few to 5 cm thick and less than a few meters long. Zone IV is characterized by massive, brown, soft rock (soil) with sporadic pale gray parts at the bottom. Zone IV is covered by black topsoil 10–20 cm thick.

Rock specimens were sampled along a horizontal sampling line crossing zones I through IV (Fig. 1). The locations of the sampling points were calculated as the depths from the original slope surface before the cutting, by assuming that the original ground surface was parallel to the planar boundary between zones II and III. From the cut surface, rock was excavated to a depth of 10–20 cm, where a nail penetration test was performed and rock specimens were sampled. Nail penetration tests were performed instead of a standardized cone penetration test or a needle penetration test because some of the rocks were too hard for these tests. A nail with a diameter of 3.4 mm was inserted vertically into the rock to a depth of 1 cm, then a metal hammer with a weight of 2.5 N was dropped vertically from a height of 80 cm within an acrylic pipe to strike the nail head. The nail was driven about an additional 3 cm into the rock with successive hammer blows, then the number of blows necessary to drive the nail the additional 3 cm (N_3) was calculated. Nail penetration test was performed once at each point. From the excavated surface, rock specimens were sampled by a portable drilling machine (for zones I and II) or by a pick and a shovel (for zones III and IV). The rock specimens were one or two cores with diameters of 5 cm and lengths of 5–10 cm or blocks with equivalent volumes.

The physical properties of bulk density, solid density, porosity and pore size distribution were measured. The measurement was made once for each sample. Each rock specimen was evacuated for 30 h in distilled water within a desiccator, then measured for its saturated weight, dried at 60 °C for 27 h, measured for its dry weight, coated by paraffin and immersed into water to measure its bulk volume. The volume of paraffin adhered to a sample was discarded from the measured volume to obtain an accurate bulk volume. In addition to these bulk volume and weight data, solid density was measured by an air-pycnometer and then used to calculate the porosity involving closed pores. Measurement error of bulk density, solid density and porosity is less than 1%. The pore size distribution was measured by the mercury-injection method using Micromeritics Pore Sizer 9320.

X-ray diffraction analysis was made using Phillips X-ray Diffractometer PW3050 for the bulk powder samples and for <2 μm fractions. X-ray fluorescence spectrometry was performed for major chemical components by using Shimazu Sequential X-ray Fluorescence Spectrometer XRF-1500PC. Loss of ignition was measured by heating the sample, which had been dried at 60 and at 750 °C for 1 hour. Heating at 60 °C was adopted instead of 110 °C to avoid the dehydration of clay minerals. The losses of ignition can be presumed to be water contents of the rock samples because they do not contain organic materials and sulfuric or carbonic compounds. Fractured rock surfaces were observed with the scanning electron microscope (SEM) Jeol T-330 equipped with an energy dispersive spectrometer.

4. Results

4.1. Physical properties and mineralogy

The number of blows necessary to drive the nail 3 cm (N_3) are plotted versus depth in Fig. 3. One N_3

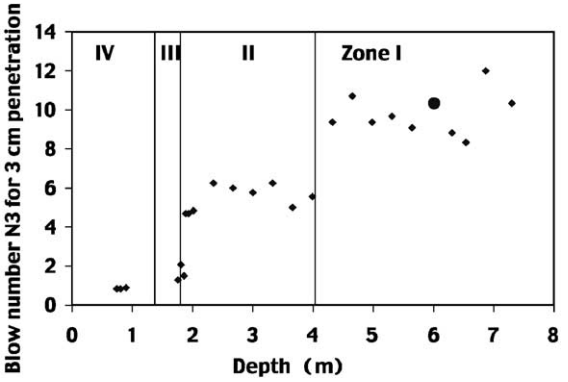

Fig. 3. Plots of blow numbers N_3. See text.

value was obtained at each point, but it is clearly seen that they change stepwise at the boundary between zones I and II and at the boundary between zones II and III. N_3 is not a common test parameter but is reasonably assumed to represent the strength of the framework of this ignimbrite.

The measured values of density, porosity and solid density are shown in Table 1 and Fig. 4, which will be discussed later. Porosity was calculated by means of two data sets: one consisting of bulk volume, bulk dry weight and bulk saturated weight, and another consisting of bulk volume, bulk dry weight and solid density. The porosities measured by these two data sets were within the range of error, suggesting that all pores are connected. The porosities of rocks from the unweathered zone were about 40%, which are within the range of rocks that experienced vapor-phase crystallization (Smith and Bailey, 1966). Porosity and density were measured for one sample at each point, so we cannot estimate their variation at each point. However, we can see their changing pattern according to the depth.

Pore size distributions are shown in Fig. 5, being arranged according to weathering zones. Their patterns are different among the weathering zones, a finding which will be discussed later.

Table 1
Physical properties of rocks according to their depths from the original ground surface and weathering zones

Zone	Depth (m)	Bulk density (g/cm^3)	Solid density (g/cm^3)	Effective porosity (%)
IV	0.6	0.93	2.45	
IV	0.74	0.97	2.48	
IV	0.89	1.23	2.50	
III	1.7	1.56	2.55	44.9
III	1.8	1.54	2.58	43.9
III	1.86	1.49	2.57	47.4
II	1.9	1.55	2.58	45.0
II	1.95	1.57	2.58	44.6
II	2.67	1.60	2.59	42.3
II	3.33	1.57	2.60	42.8
II	3.99	1.67	2.60	38.9
I	4.65	1.69	2.63	40.0
I	5.31	1.69	2.64	37.2
I	5.97	1.69	2.63	38.6
I	6.64	1.67	2.64	38.8

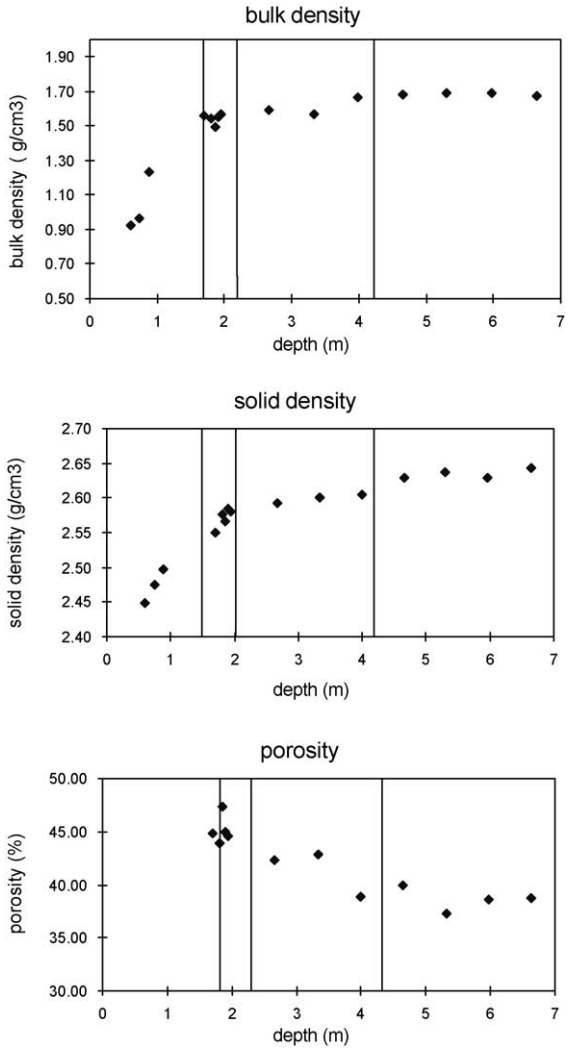

Fig. 4. Plots of the physical properties of rocks according to their depth from the original ground surface and weathering zones.

The minerals identified by the X-ray diffraction analysis of bulk samples were quartz, feldspar, hornblende, pyroxene, cristobalite and tridymite. Smectite was detected locally as weak diffraction peaks from <2 μm fractions. The qualitative amounts suggested by the reflection intensities of these minerals are shown in Table 2. Among these minerals, cristobalite, tridymite, hornblende and feldspar in particular changed their amounts significantly with respect to the weathering zones, as will be discussed later.

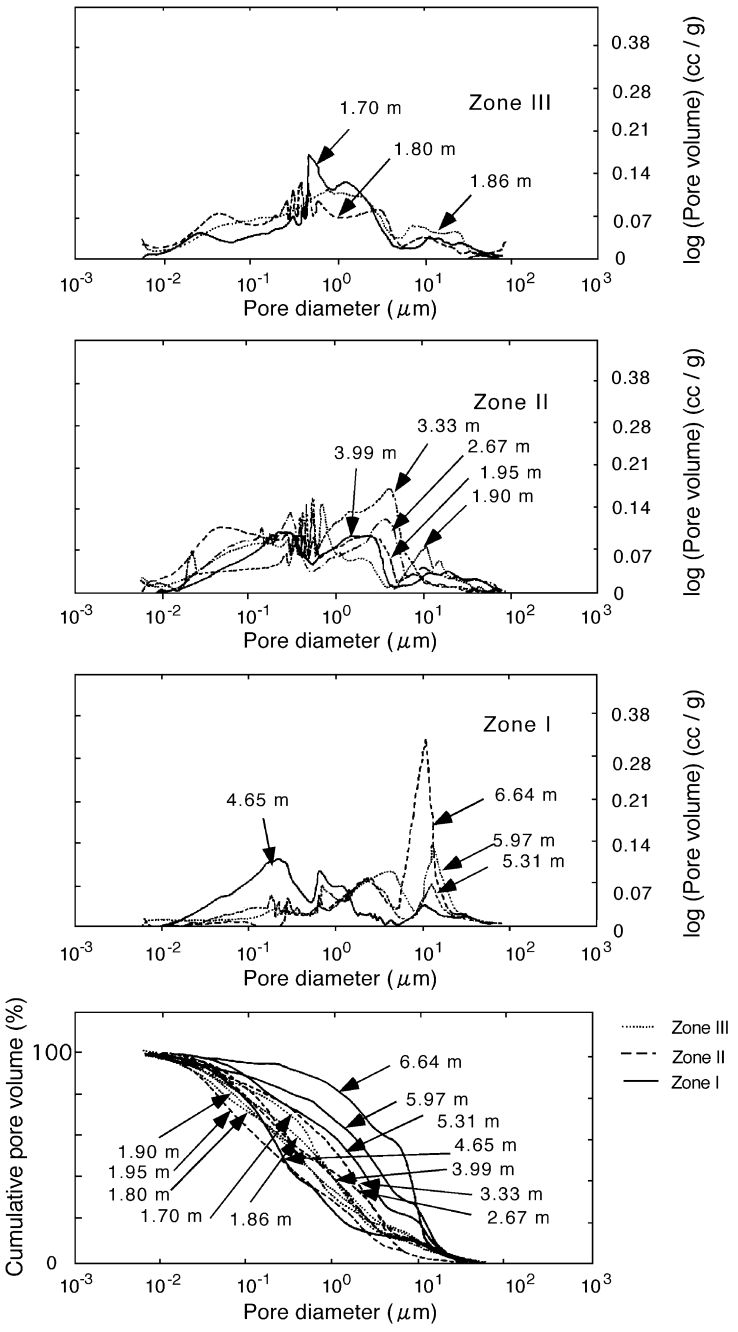

Fig. 5. Plots of the pore size distribution of rocks according to their depth from the original ground surface and weathering zones.

Table 2
Qualitative amounts of minerals indicated by the X-ray diffraction peaks of each minerals

Zone	Depth (m)	Quartz	Feldspar	Pyroxene	Hornblend	Smectite	Cristobalite	Tridymite
IV	0.6	++	+	–	–		+	–
IV	0.74	++	+	–	–	–	+	(+)
IV	0.89	++	+	+	(+)		+	–
III	1.7	+++	++	+	(+)	–	+++	–
III	1.8	+++	++	+	(+)	–	+++	–
III	1.86	+++	++	+	(+)	–	+++	–
II	1.9	+++	+++	+	+	–	++	–
II	1.95	+++	+++	+	+	–	++	–
II	2.67	+++	+++	+	+	(+)	++	–
II	3.33	+++	+++	+	+	–	++	–
II	3.99	+++	+++	+	+	(+)	++	–
I	4.65	+++	+++	+	+	(+)	+	+
I	5.31	+++	+++	+	+	(+)	(+)	++
I	5.97	+++	+++	+	+	–	(+)	++
I	6.64	+++	+++	+	+	–	(+)	++

+++: strong reflection; ++: moderate; +: weak; (+): very weak; – : no reflection

4.2. Gain or loss of chemical elements, volumetric change and change of mass

The chemical compositions measured are shown in Table 3. In order to elucidate the behavior of chemical elements during the weathering, the volume, mass and amounts of the chemical constituents have been compared before and after the weathering. Ti is the most immobile of the major constituent elements and hence has been used for the analysis of chemical change during metamorphism and weathering (Isocon diagram of Grant, 1986; Chigira, 1998; Guan et al., 2001). The basis of the calculation is as follows. TiO_2 content in a given volume of rock is presented as $\rho_0 V_0 C_{Ti(0)}$ and $\rho_1 V_1 C_{Ti(1)}$ before and after weathering, respectively, in which ρ, V and C_{Ti} are bulk density, bulk volume of a given element and Ti concentration, respectively. The suffixes 0 and 1 represent before and

Table 3
Chemistry of samples according to the depths from the original ground surface; chemical compositions of the collected samples (wt.%)

Zone	Depth (m)	SiO2	TiO2	Al2O3	Fe2O3	MnO	MgO	CaO	Na2O	K2O	P2O5	Ig. Loss
IV	0.6	50.82	0.88	21.23	9.74	0.13	2.93	1.73	1.05	0.92	0.08	10.48
IV	0.74	49.67	0.87	21.48	9.66	0.13	2.76	1.63	1.07	0.94	0.08	11.70
IV	0.89	56.68	0.71	19.64	7.74	0.11	2.27	2.19	1.53	1.08	0.06	7.99
III	1.7	69.63	0.44	16.01	3.83	0.07	0.55	2.44	1.73	0.84	0.02	4.43
III	1.8	69.47	0.42	16.18	3.74	0.06	0.43	2.39	1.79	0.91	0.03	4.59
III	1.86	67.87	0.43	17.32	3.35	0.05	0.50	2.67	1.96	0.88	0.02	4.95
II	1.9	70.14	0.43	16.40	3.61	0.06	0.51	2.58	1.87	0.96	0.02	3.42
II	1.95	68.91	0.42	16.38	3.63	0.07	0.52	2.77	2.19	1.27	0.03	3.81
II	2.67	71.58	0.41	14.59	3.26	0.07	0.61	3.02	2.30	1.33	0.03	2.81
II	3.33	70.20	0.38	15.78	3.28	0.06	0.50	3.20	2.50	1.38	0.02	2.70
II	3.99	70.05	0.37	15.58	3.30	0.07	0.56	3.27	2.69	1.47	0.03	2.61
I	4.65	70.18	0.38	15.64	3.24	0.06	0.51	3.46	2.99	1.55	0.06	1.93
I	5.31	70.43	0.39	15.26	3.36	0.07	0.61	3.49	3.17	1.52	0.06	1.66
I	5.97	71.73	0.36	14.71	3.21	0.06	0.53	3.42	3.22	1.48	0.06	1.21
I	6.64	71.79	0.39	14.63	3.27	0.06	0.54	3.35	3.21	1.52	0.07	1.16

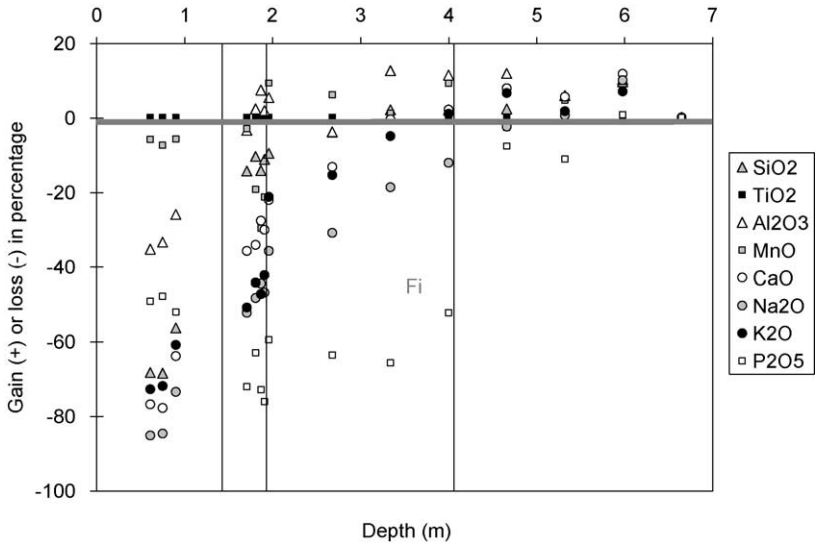

Fig. 6. Loss of alkali, alkali earth, phosphorus, silica, aluminum and manganese by weathering.

after weathering, respectively. Equalizing the amounts of Ti within the volume before and after weathering and rearranging the equation, we obtain

$$V_1/V_0 = \rho_0 C_{\mathrm{Ti}(0)}/\rho_1 C_{\mathrm{Ti}(1)}.$$

When the masses of the volume before and after weathering are shown by $M_{s(0)}$ and $M_{s(1)}$, the change in mass is represented by

$$(M_{s(0)} - M_{s(1)})/M_{s(0)} = (\rho_0 V_0 - \rho_1 V_1)/\rho_0 V_0$$
$$= 1 - (\rho_1/\rho_0)(V_1/V_0).$$

The relative loss of a chemical constituent i is represented by

$$(M_{i(0)} - M_{i(1)})/M_{i(0)}$$
$$= (\rho_0 V_0 C_{i(0)} - \rho_1 V_1 C_{i(1)})/\rho_0 V_0 C_{i(0)}$$
$$= 1 - (\rho_1/\rho_0)(C_{i(1)}/C_{i(0)})(V_1/V_0)$$
$$= 1 - (\rho_1/\rho_0)(C_{i(1)}/C_{i(0)})(\rho_0 C_{\mathrm{Ti}(0)}/\rho_1 C_{\mathrm{Ti}(1)})$$
$$= 1 - (C_{i(1)}/C_{i(0)})(C_{\mathrm{Ti}(0)}/C_{\mathrm{Ti}(1)})$$

The calculated results of the volume change or chemical gain or loss from the rock which was taken from

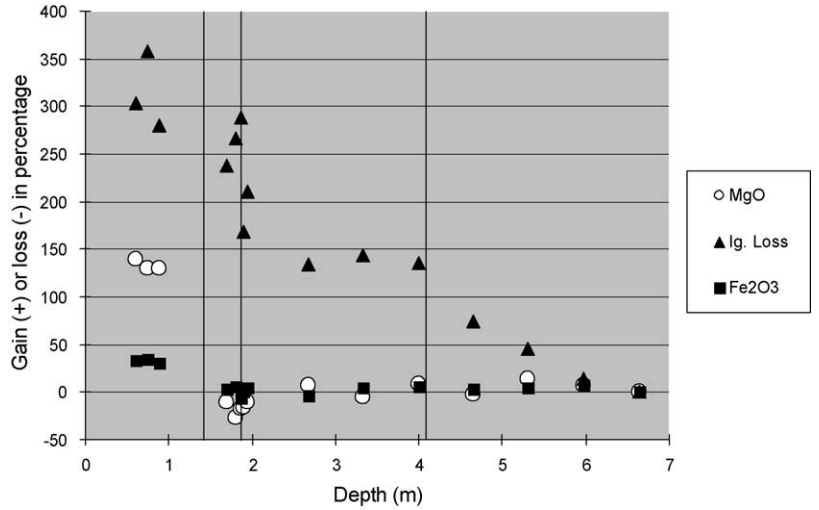

Fig. 7. Gain of ignition loss (H_2O), iron and magnesium by weathering.

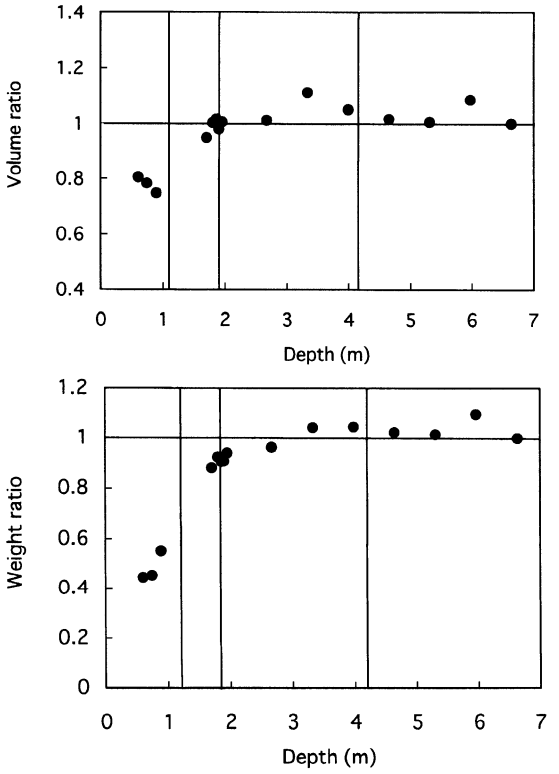

Fig. 8. Volume change and weight change by weathering.

the deepest zone are shown in Figs. 6, 7 and 8, and will be discussed in the following sections.

5. Discussion

5.1. Geological characteristics of the weathering zones and the fronts

On the basis of the analytical results described above, three weathering fronts and three corresponding weathering sub-zones are characterized. The physical, mineralogical and chemical properties change mostly stepwise, defining the weathering fronts and the weathering zones between them.

5.1.1. Hydration front and hydrated zone

Zone II is characterized by hydration, softening, the disappearance of tridymite and the formation of cristobalite and the depletion of P_2O_5, Na_2O, K_2O and CaO. The water contents represented by the loss of ignition indicate that hydration occurs at the base of zone II and also slightly in the transitional zone just beneath it, and that the water content within zone II is essentially constant except for its top (Fig. 7). This is the most important characteristic of this zone, because hydration is closely related to other chemical changes and to the change in physical properties. Therefore, this zone is called the hydrated zone, and its base is called the hydration front. The transitional zone beneath this front is assumed to be transitional, because the water content decreases downward to become constant within a few meters from this front.

The X-ray reflection profiles of rocks from zone I had two peaks around 22° of 2θ (CuKα) (Fig. 9). One is of tridymite (002) and the other is of cristobalite (101) (Jones and Segnit, 1971; Florke et al., 1990); tridymite and cristobalite are common minerals of the vapor-phase crystallization of ignimbrite (Cas and Wright, 1996; Yurtmen and Rowbotham, 1999). As is seen in Fig. 9, the tridymite peaks get weak near the boundary between zones I and II and disappear at this boundary, while cristobalite peaks, in turn, get stronger there. These changes in the reflection patterns indicate that tridymite is depleted and cristobalite is formed around the boundary between zones I and II. SEM observation indicates that platy tridymite crystallites are dissolved and cristobalite particles precipitate in the interstices (Fig. 10). This dissolution and

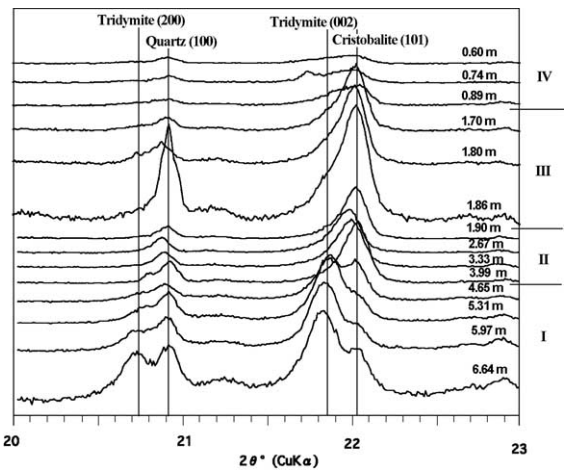

Fig. 9. X-ray deflection profiles showing the peaks of cristobalite and tridymite.

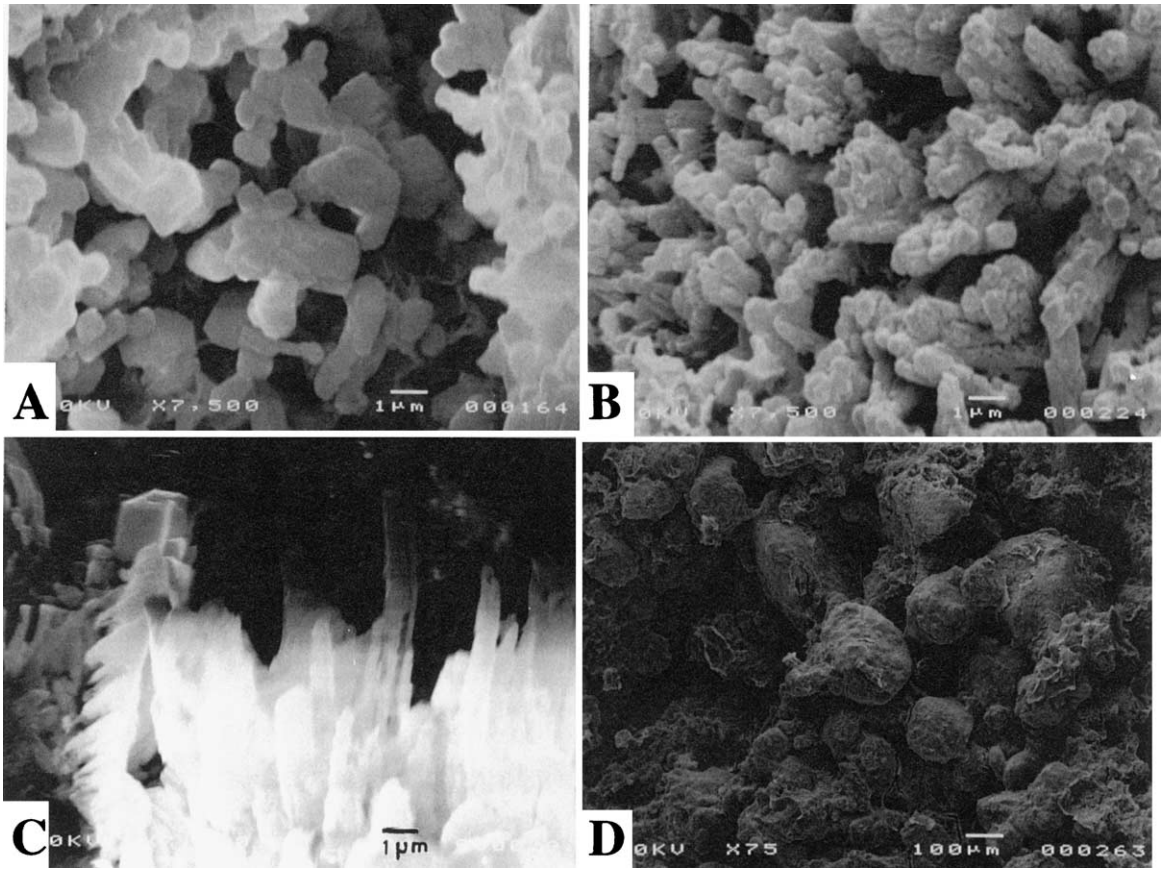

Fig. 10. Scanning electron microscope images of the rock matrices of each zone. (A) Tridymite grains in zone I (6.64 m). (B and C) Dissolved tridymite pseudomorphs in zones II (3.33 m) and III (1.8 m). (D) Particles enveloped by a film containing iron in zone IV (0.6 m).

precipitation is probably due to the fact that tridymite is more soluble than cristobalite (Dove and Rimstidt, 1994). Cristobalite and tridymite have been known to precipitate as metastable minerals under earth surface conditions (Jones and Senit, 1972).

Phosphorus was calculated to be leached by more than 50% at this front (Fig. 6), although its chemical and mineral species are not known. Na_2O, K_2O and CaO decrease more in the shallower part within this zone.

Significant softening occurs at this front, as is shown by the nail blow numbers (Fig. 3). This softening is due to the breakage of the interconnection of the tridymite crystallites that had been supporting the framework of the ignimbrite (Fig. 10A,B).

Porosity increases from 39% to 42% within an interval of 70 cm above this front (Fig. 4). Solid density decreases slightly from 2.64 to 2.60 g/cm^3 at this front.

Pore sizes decrease just beneath this front (Fig. 5). A 10-μm peak in pore size distribution becomes weaker and 3–5 μm peaks become stronger. D50 diameters get smaller from 2–10 to 0.2–1 μm.

This zone accompanies a thin zone at its top, which is transitional from zone II to the overlying zone III. The transitional zone is not separated from the hydrated zone by a fracture, but is a precursor of the thin slabs in zone III. The properties of rocks within this transitional zone will be discussed with those of zone III.

5.1.2. Exfoliation front and exfoliated zone

Zone III is characterized by the softening and exfoliation of rock, and is called the exfoliated zone; its base is the exfoliation front. The rock structure

changes from the massive rock of the hydrated zone to the assemblage of platy rocks of the exfoliated zone. The blow number N_3 decreases stepwise at this front (Fig. 3). However, significant changes in chemical properties occur just beneath the front (Figs. 6 and 7). The interval in which chemical properties change is less than 10 cm thick and is called the transitional zone. H_2O, which is constant within the main part of the hydrated zone, increases again within the transitional zone. Alkali and alkali earth elements are leached by 10–20% within this transitional zone, and in smaller amounts within the exfoliated zone. Porosity increases by 3% from 42% to 45%, but the change in solid density is slight (Fig. 4). The peak of the pore size distribution curve shifts to around 1 μm. D50 diameters are 0.4–0.8 μm, within the same range as those of zone II (Fig. 6). Rock softening occurs slightly at the transitional zone and proceeds significantly at the exfoliation front. Matrix-forming materials of a probable pseudomorph of tridymite crystallite are no longer in platy shape but are of irregularly shaped bullet nose (Fig. 10C).

5.1.3. Disintegration front and disintegrated zone

Zone IV is characterized by the complete disappearance of rock structure, intensive leaching of many elements except for water, iron and magnesium, and the reduction of rock volume. This zone is called the disintegrated zone and its base is called the disintegration front, but is also known as the oxidation front because of the brownish color of this zone and the gray color beneath this front.

Rock structure changes drastically from the underlying exfoliated zone. The rock slabs of zone III decrease their size near its top and disappear in the disintegrated zone. The boundary between these two zones is gradual within an interval of 10–20 cm. The rock matrix observed under the SEM has completely changed its structure from the framework structure of tridymite pseudomorphs to the assemblage of small particles surrounded by amorphous films containing iron (Fig. 10D). The cristobalite peaks of the X-ray reflection profile become very weak and broad (Fig. 9), indicating that it decreases substantially.

The rock strength represented by the blow numbers needed for nail penetration is the same as that of rock in the exfoliated zone (Fig. 3). The bulk and solid density decrease substantially from those of the rocks in the exfoliated zone, the former from 1.5 to 1 g/cm^3 and the latter from 2.6 to 2.5 g/cm^3 (Fig. 4). Scanning electron microscopy suggests that porosity also increases at this front, although the exact values were not measured; the material constituting this zone was too weak to be used for the pore-size analysis. Rock volume is estimated to have decreased at this front by 20% on the basis of the calculation of chemical loss and gain (Fig. 8).

Silicon and aluminum, which are not leached in the underlying zones, are leached in this zone as well as alkali and alkali earth elements (Fig. 6). H_2O, iron and magnesium content increase in this zone (Fig. 7). Magnesium and iron are probably derived from the topsoil that was not analyzed in this study. Pyroxene and hornblende are depleted, and feldspar, quartz and cristobalite also decrease (Table 2).

5.2. Weathering mechanism of the ignimbrite consolidated by vapor-phase crystallization

Zones II, III and IV are arranged from the depth to the ground surface in this order, and the weathering proceeds by the downward migration of these weathering zones. Zone I, which is fresh zone, changes to zone II, zone II to zone III, and zone III to zone IV. These changes occur primarily through chemical processes, particularly the interaction of interstitial water and rock. The interactions between the infiltrating water and the rocks in the weathering zones are described from the ground surface downward, based on the analytical results described in the preceding sections (Fig. 11). First, rainwater goes down through topsoil, acquiring biogenic carbon dioxide within the topsoil. The water, slightly acidic and highly reactive because of its dilute nature, reaches the disintegration front, where it interacts with the rock of the exfoliated zone, completely breaking the rock texture and leaching even less mobile components such as aluminum and silica, as well as alkali and alkali earth elements. The silica mineral, cristobalite, which survived the leaching within the exfoliated zones, decreases significantly at this front. These chemical reactions concentrate in the disintegration front.

Water that penetrates the disintegration front further infiltrates through the exfoliated zone downward, reaching the base of the exfoliated zone. The water within this zone and also the above disintegrated zone

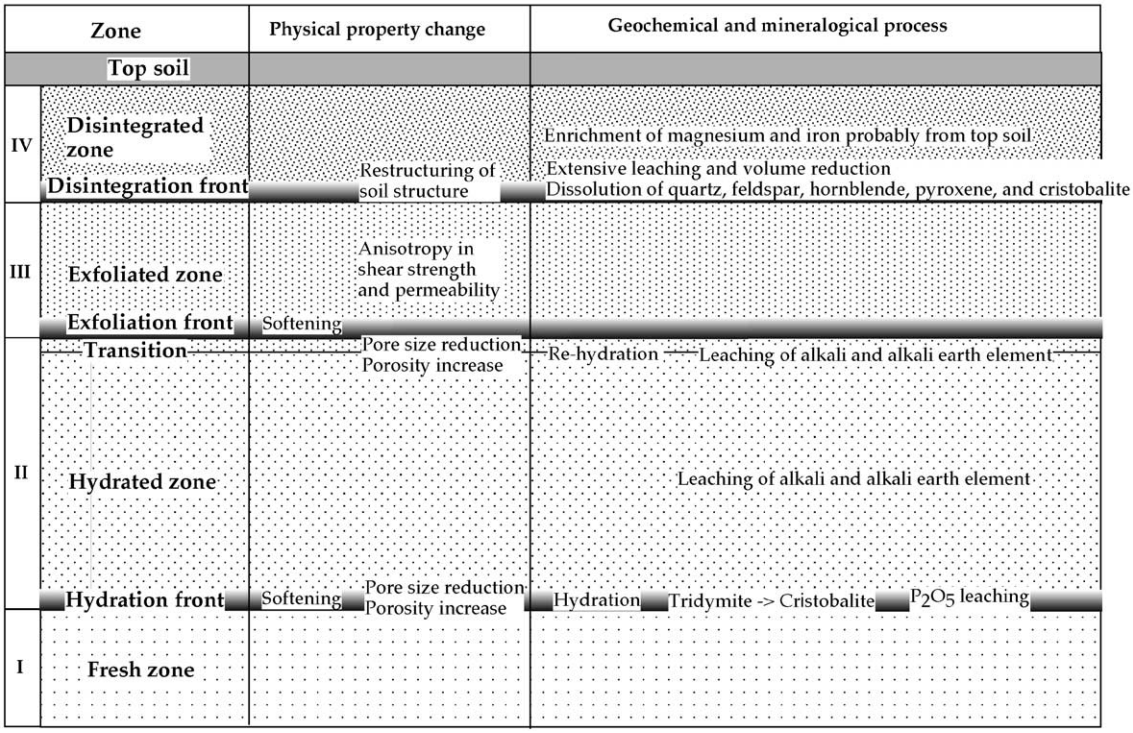

Fig. 11. Schematic sketch showing the weathering mechanisms of the ignimbrite consolidated by vapor-phase crytallization.

moves relatively quickly and is refreshed frequently in comparison with the water within the underlying hydrated zone because the rocks of the former two zones are far more permeable than the rock of the hydrated zone. At the base of the exfoliated zone, this relatively reactive water contacts the underlying rock of the transitional zone just beneath the exfoliated zone. The groundwater flows along the exfoliation front, extracting and transporting the chemical components such as alkali and alkali earth elements from the transitional zone. Silica within the rock is not leached out, because the water is probably nearly saturated with cristobalite, by virtue of the dissolution of cristobalite at the disintegration front. The leaching results in the deterioration of the rock in the transitional zone, which would be separated from the hydrated zone to become a member of the exfoliated zone. The separation may be caused by volumetric strain due to the iteration of drying and wetting of the rock.

Water passes through the exfoliated zone and the underlying transitional zone, infiltrating downward more slowly than in the zones above because of the absence of cracks and the low permeabilities of the rock matrices. The groundwater leaches out alkali and alkali earth elements within the hydrated zone, leaching more in the shallower part. The water reaches the hydration front, where hydration and the leaching of phosphorus occur, although the chemical forms of the hydration water and the phosphorus are not known. Tridymite, which has a greater solubility than cristobalite (Dove and Rimstidt, 1994), disappears around this front, and probably transforms into cristobalite by a dissolution precipitation reaction.

The groundwater penetrates only slightly through the hydration front, as shown by the graph of chemical change (Fig. 7). Fig. 7 shows that the water content is increased only slightly within an interval of a few meters beneath the front. This interval might be a zone of accidental wetting. Ordinarily, the zone could be kept dry by the following hydraulic barrier brought about by the arrangement of a bed with smaller pore sizes on a bed with larger pore sizes. The pore sizes were smaller in the hydrated and exfoliated zones than in the fresh zone; the D50 diameters of the pores were

0.2–1 μm within the hydrated and exfoliated zones and 2–10 μm within the fresh zone. There were also fewer larger pores in the weathering zones than in the fresh zone. This difference in pore sizes might result in the water within the hydrated zone not infiltrating downward because of the higher capillary force within the hydrated zone than in the underlying fresh zone. The height of the fringe zone within the hydrated zone, which is calculated from the capillary tension and pore sizes (Iwata et al., 1988), could be about 150–30 m, much higher than the level of the overlying weathering zones (the exfoliated and disintegrated zones). These heights are calculated with the assumption that the pores are simple cylindrical tubes with uniform diameters, so that the fringe height in nature would be somehow different.

5.3. Weathering profile and landslide generation

In considering the landslide generation of the 1998 rainstorm, the most important characteristic of the weathering profile was the presence of the exfoliated zone just above the massive hydrated zone. First, the exfoliation surfaces dip downslope parallel to the slope surface, providing a dip slope. In addition, the shear strength along the exfoliation surface is estimated to be very low because of the weakness of the rock, which is represented by nearly the same nail-penetration blow numbers (N_3) as those of the soil in the disintegrated zone. The weathering profile thus provides slopes that are mechanically preferable for a landslide. Hydraulic conditions that are also favorable for landslide generation are provided by the weathering profile. Water from the rain goes down through the interstitial pores in the disintegrated zone and along the exfoliation fractures in the exfoliated zone, but cannot penetrate into the hydrated zone because its rock is less permeable and also because the water pressure within the hydrated zone might not be large enough to break the capillary tension at the base of this zone. The water, therefore, would flow laterally within the exfoliated and disintegrated zones, which would become saturated if the rainfall were intensive enough. Plant roots, which could be a reinforcement against landsliding, are limited to the disintegrated and the exfoliated zones and do not penetrate into the underlying hydrated zone because of the absence of cracks, so they support the weathered rocks only laterally.

The weathering of this type of ignimbrite thus changes its structure and properties so that the weathered material slides easily. This means that the ignimbrite has a special type of denudation process that includes weathering and landslide. First, the weathering fronts migrate downward and the weathering zone extends into the depth. After the weathering zone becomes thick enough to slide, a rainstorm may trigger the slide by saturating the weathered material, or an earthquake may generate sliding. Weathering is thus followed by the descent of the ground surface by landsliding. In fact, the exfoliated and disintegrated zones at the outcrop under study had partly slid as a result of the heavy rain of August 1998. In addition, many of the landslide scars generated by the rainstorm had slip surfaces within the exfoliated zone. The landslides stripped off the major part of the exfoliated zone and the overlying disintegrated zone and left some rock slabs of the exfoliated zone at the scars. After the landslide, weathering commenced again to form the mature weathering profile as described above. However, the weathering rate is not known at present.

This paper clarified that the ignimbrite that is consolidated by vapor-phase crystallization, or at least Shirakawa pyroclastic flow, is weathered with the exfoliated zone at the bottom of the heavily weathered part, and that this zone is very sensitive to rainstorms and reasonably sensitive to earthquakes. However, this is not the case for non-welded and unconsolidated ignimbrite, such as Shirasu, whose weathering profile lacks an exfoliated zone and an exfoliation front (Yokota and Iwamatsu, 1999). This difference in weathering profiles must reflect the fact that the vapor-phase crystallization devitrifies glass fragments and precipitates tridymite and cristobalite, which consolidate the ignimbrite, whereas non-welded and unconsolidated ignimbrite consists mainly of glass fragments. This difference in the weathering profile would generate the difference in the rainfall patterns that generate landslide.

6. Conclusions

The Shirakawa pyroclastic flow, one of the typical ignimbrites consolidated by tridymite and cristobalite under vapor-phase crystallization, has a special type

of weathering profile, which provided the basic causes for numerous landslides that occurred as a result of the rainstorm of August 1998, in Fukushima Prefecture, Japan. The profile consists of the topsoil, the disintegrated zone (which is like soil), the exfoliated zone and the massive, hydrated zone from the ground surface to the depth. The bases of these zones are the disintegration front, exfoliation front and hydration front, respectively. Rainwater infiltrates through the topsoil and reaches the disintegration front, where it interacts with the rock of the exfoliated zone, completely breaking the rock texture and leaching even less mobile components, such as aluminum and silica, as well as alkali and alkali earth elements. Water further infiltrates through the exfoliated zone, where rock is exfoliated into slabs ranging from a few centimeters to 5 cm thick, and reaches the exfoliation front, extracting and transporting the chemical components, such as alkali and alkali earth elements from the transitional zone just beneath the front. The leached layer of the transitional zone is finally exfoliated from the hydrated zone to be a member of the exfoliated zone. Water that has passed through the exfoliated zone infiltrates downward far more slowly to leach alkali and alkali earth elements and phosphorous from the rock in the hydrated zone. Tridymite is transformed into cristobalite around the hydration front. Groundwater infiltrates easily down to the exfoliation front but with more difficulty beneath it, so that a heavy rainstorm would saturate the weathering zone above the exfoliation front. Thus, saturated weathered materials slid in many locations with slip surfaces within the exfoliated zone as a result of the 1998 rainstorm in Nishigo Village, northern Japan.

References

Best, M.G., Christinsen, E.H., 2001. Igneous Petrology. Blackwell, Massachusetts.

Cas, R.A.F., Wright, J.V., 1996. Volcanic Successions: modern and Ancient. Allen and Unwin, London.

Chigira, M., 1998. An Introduction to Hazard Geology. Kinmiraisha, Nagoya.

Chigira, M., Inokuchi, T., 1998. Landslides triggered by August 1998 heavy rainfall, northern Japan. Landslide News, in press.

Dove, P.M., Rimstidt, J.D., 1994. Silica–water interactions. In: Heaney, P.J., Prewitt, C.T., Gibbs, G.V. (Eds.), Silica and Physical Behavior, Geochemistry and Materials Applications. Mineralogical Society of America, Washington, D.C., pp. 256–308.

Florke, O.W., Graetsch, H., Jones, J.B., 1990. Hydrothermal deposition of cristobalite. N. Jb. Miner. Mh. H.2, 81–95.

Grant, J.A., 1986. The isocon diagram—a simple solution to Gresens' equation for metasomatic alteration. Econ. Geol. 81, 1976–1982.

Guan, P., Ng, C.W.W., Sun, M., Tang, W., 2001. Weathering indices for rhyolitic tuff and granite in Hong Kong. Eng. Geol. 59, 147–159.

Iwata, S., Taguchi, T., Warkentin, B.P., 1988. Soil–Water Interactions. Dekker, New York.

Jones, J.B., Segnit, E.R., 1971. The nature of opal: I. Nomenclature and constituent phases. J. Geol. Soc. Aust. 18, 57–68.

Jones, J.B., Senit, E.R., 1972. Geneis of cristobalite and tridymite at low temperatures. J. Geol. Soc. Aust. 18, 419–422.

Olsen, H.W., Nichols, R.W., Rice, T.L., 1985. Low gradient permeability measurements in a triaxial system. Geotechnique 35, 145–157.

Saotome, H., Research Group of the August 27 disaster, 1999. Types of landslides occurred during the August 27 disaster of in the south of Fukushima Prefecture, 1998. Proceedings of the 18th Conference of the Japan Society for Natural Disaster Science, 7–8.

Shimokawa, E., Jitouzono, T., Takano, S., 1989. Periodicity of shallow landslide on Shirasu (Ito pyroclastic flow deposits) steep slopes and prediction of potential landslide sites. Trans., Jpn. Geomorphol. Union 10, 267–284.

Smith, R.L., Bailey, R.A., 1966. The Bandelier Tuff, a study of ash-flow eruption cyles from zoned magma chambers. Bull. Volcanol. 29, 83–104.

Suzuki, T., 1999. Tephrochronological study on Nasu volcano. Bull. Volcanol. Soc. Jpn. 37, 251–263.

Suzuki, T., Fujiwara, O., Danhara, T., 1998. Fission track ages of eleven Quaternary Tephras in north Kanto and south Tohoku regions, central Japan 37, 95–106, Ushiyama.

Ushiyama, M., 1999. Characteristics of heavy rainfall in Tochigi and Fukushima Prefectures on August 26–31, 1998. J. Jpn. Soc. Nat. Disaster Sci. 17, 237–244.

Yokota, S., Iwamatsu, A., 1999. Weathering distribution in a steep slope of soft pyroclastic rocks as an indicator of slope instability. Eng. Geol. 55, 57–68.

Yokoyama, S., 1999. Rapid formation of river terraces in non-welded ignimbrite along the Hishida Riber, Kyushu, Japan. Geomorphology 30, 291–304.

Yoshida, H., Takahashi, M., 1991. Geology of the eastern part of the Shirakawa pyroclastic flow field. J. Geol. Soc. Jpn. 97, 231–249.

Yurtmen, S., Rowbotham, G., 1999. A scanning electron microscope study of post-depositional changes in the northeast Nigde ignimbrites, South Central Anatolia, Turkey. Mineral. Mag. 63, 131–141.